The role of spatial variations of abiotic factors in mediating intratumour phenotypic heterogeneity

Keywords: Intratumour heterogeneity | Phenotypic selection | Mathematical oncology | Partial differential equations | Finite element methods

Authors: Tommaso Lorenzi[1†], Chandrasekhar Venkataraman[1†], Alexander Lorz[2,3] and Mark A.J. Chaplain[1].

[†] These primary authors contributed equally to this paper.

Author's Affiliations: [1] School of Mathematics and Statistics, University of St Andrews, St Andrews KY16 9SS, United Kingdom; [2] CEMSE Division, King Abdullah University of Science and Technology (KAUST), Thuwal, Saudi Arabia; [3] Sorbonne Universités, UPMC Univ Paris 06, UMR 7598, Laboratoire Jacques-Louis Lions, Paris, France.

Corresponding Author: Mark A.J. Chaplain, E-mail: majc@st-andrews.ac.uk, School of Mathematics and Statistics, University of St Andrews, St Andrews KY16 9SS, United Kingdom.

Abstract

A growing body of evidence indicates that the progression of cancer can be viewed as an eco-evolutionary process. Under this perspective, we present here a space- and phenotype-structured model of selection dynamics between cancer cells within a solid tumour. In the framework of this model, we combine formal analyses with numerical simulations to investigate *in silico* the role played by the spatial distribution of abiotic components of the tumour microenvironment in mediating phenotypic selection of cancer cells. Numerical simulations are performed both on the 3D geometry of an *in silico* multicellular tumour spheroid and on the 3D geometry of an *in vivo* human hepatic tumour, which was imaged using computerised tomography. The results obtained show that inhomogeneities in the spatial distribution of oxygen, currently observed in solid tumours, can promote the creation of distinct local niches and lead to the selection of different phenotypic variants within the same tumour. This process fosters the emergence of stable phenotypic heterogeneity and supports the presence of hypoxic cells resistant to cytotoxic therapy prior to treatment. Our theoretical results demonstrate the importance of integrating spatial data with ecological principles when evaluating the therapeutic response of solid tumours.

Introduction

Significant progress in understanding the mechanisms behind cancer development and progression has been achieved in recent years by using molecular-based sequencing techniques [1–7]. Despite this growing knowledge, we are far from a complete understanding of the principles that govern the emergence of intratumour heterogeneity. This poses a major obstacle to successful cancer chemotherapy and management of disease relapse [8–10].

A novel perspective on cancer therapeutics can be obtained from the accumulating evidence indicating that the progression of solid tumours is, in essence, an eco-evolutionary process [11–13]. Firstly, new phenotypic variants emerge in the tumour via mutations and epimutations. Afterwards, these variants are subject to natural selection and they proliferate and die under the selective pressures of the tumour microenvironment. From this evolutionary viewpoint, spatial variations in the distribution of abiotic components of the tumour microenvironment (*e.g.*, nutrients and therapeutic agents) may lead to the creation of distinct local niches and thus provide ecological opportunities for diversification [14–17].

To explore *in silico* the validity of such an ecological argument linking heterogeneity in the distribution of abiotic components of the tumour microenvironment to the development and maintenance of phenotypic heterogeneity between cancer cells, we present here a space- and phenotype-structured model of selection dynamics in a solid tumour. Our model consists of an integro-differential equation (IDE) for the spatiotemporal evolution of the phenotypic distribution of cancer cells [18–21] coupled to a system of partial differential equations (PDEs) for the dynamics of abiotic factors [22–24].

Recent studies based on various mathematical modelling approaches support related hypotheses concerning the emergence of intratumour heterogeneity. For instance, Fu *et al.* [25] have proposed a model based on a multi-type stochastic branching process describing growth of cancer cells in multiple spatial compartments characterised by different environmental conditions. Further, Lorz *et al.* [26] have developed an IDE model of phenotypic selection in a radially symmetric tumour spheroid viewed as a population structured by a phenotypic trait and a 1D spatial variable. More recently, Lloyd *et al.* [27] have considered an evolutionary game theory model of habitat heterogeneity where the tumour is composed of two compartments – the tumour core and the tumour edge – treated as two different habitats. Although these studies provide a valuable proof of concept for the hypothesis that spatial gradients of abiotic factors cause the selection of different phenotypic properties in distinct regions within the same solid tumour, they are based on mathematical models that rely on rather strong simplifying modelling assumptions. On the contrary, our mathematical model requires no specific assumptions on the tumour geometry, and its parameters can be linked to experimentally measurable quantities. For these reasons, the model presented here offers a more flexible and realistic mathematical framework for studying phenotypic selection between cancer cells within solid tumours.

In this paper, integrating the results of formal analyses with numerical simulations, we show that inhomogeneities in the spatial distribution of oxygen, which are recurrently observed in solid tumours, can promote the creation of distinct local niches and lead to the selection of different phenotypic variants within the same tumour. This process fosters the emergence of stable phenotypic heterogeneity and supports the presence of hypoxic cells resistant to cytotoxic therapy prior to treatment. Moreover, our theoretical results reveal how intratumour heterogeneity can reduce the efficacy of cytotoxic drugs, leading to poor treatment outcomes, and demonstrate the importance of integrating spatial data with ecological principles when evaluating the therapeutic response of solid tumours.

Model description

We identify the tumour geometry with a spatial domain $\Omega \subset \mathbb{R}^3$. At time t and for each point $\mathbf{x} \in \Omega$, the function $n(t, \mathbf{x}, y) \geq 0$ describes the phenotypic distribution of cells. The vector $\mathbf{x}$ denotes the position in the tumour and the continuous scalar variable $y \in [0, 1]$ represents the normalised expression level of a hypoxia-responsive gene [28, 29]. Cells within the tumour proliferate and die due to competition for limited space. Moreover, a cytotoxic drug can be administered which acts by increasing the death rate of cells. We assume increasing values of the phenotypic state y to be correlated with a progressive switch towards a hypoxic phenotype, which, in turn, implies a progressive reduction in the proliferation rate [27, 30]. Additionally, given that cytotoxic agents target mostly rapidly proliferating cells, we assume higher values of the phenotypic state y correspond to higher levels of resistance to the cytotoxic drug [31, 32].

Given the local population density of cells in the tumour $n(t, \mathbf{x}, y)$, we define the local density of cells $\rho(t, \mathbf{x})$ and the total number of cells $N(t)$ as follows

$$\rho(t, \mathbf{x}) = \int_0^1 n(t, \mathbf{x}, y) \, \mathrm{d}y, \qquad N(t) = \int_\Omega \rho(t, \mathbf{x}) \, \mathrm{d}\mathbf{x}. \tag{1}$$

The mean cell phenotypic state at position $\mathbf{x}$ and time t can be computed as

$$\mu(t,\mathbf{x}) = \frac{1}{\rho(t,\mathbf{x})} \int_0^1 y\, n(t,\mathbf{x},y)\,\mathrm{d}y. \tag{2}$$

Finally, we introduce the functions $s(t,\mathbf{x}) \geq 0$ and $c(t,\mathbf{x}) \geq 0$ to model the local concentration of oxygen and cytotoxic drug at position $\mathbf{x}$ and time t, respectively.

Dynamics of cancer cells

The dynamics of the local population density $n(t,\mathbf{x},y)$ is governed by the following nonlinear IDE

$$\frac{\partial n}{\partial t}(t,\mathbf{x},y) = R\big(y,\rho(t,\mathbf{x}),s(t,\mathbf{x}),c(t,\mathbf{x})\big)\; n(t,\mathbf{x},y). \tag{3}$$

In (3), the function $R\big(y,\rho(t,\mathbf{x}),s(t,\mathbf{x}),c(t,\mathbf{x})\big)$ represents the fitness of cells with phenotypic state y at position $\mathbf{x}$ and time t, given the local environmental conditions . These are determined by the local cell density $\rho(t,\mathbf{x})$ as well as by the concentrations of abiotic factors $s(t,\mathbf{x})$ and $c(t,\mathbf{x})$. Throughout the paper, we define the fitness landscape of the tumour as

$$R\big(y,\rho(t,\mathbf{x}),s(t,\mathbf{x}),c(t,\mathbf{x})\big) = p(y,s(t,\mathbf{x})) - k(y,c(t,\mathbf{x})) - d\rho(t,\mathbf{x}). \tag{4}$$

The definition given by (4) relies on the idea that a higher cell density $\rho(t,\mathbf{x})$ at position $\mathbf{x}$ corresponds to a more intense competition for space. We assume cells located at position $\mathbf{x}$ die with rate $d\rho(t,\mathbf{x})$, where the parameter $d > 0$ represents the death rate due to intratumour competition between cells. The function $k(y,c) \geq 0$ models the additional death rate due to the cytotoxic drug. Since increasing values of the phenotypic state y correspond to higher levels of cytotoxic-drug resistance, we assume the function k to be decreasing in y. Moreover, since the death rate increases with higher drug concentrations, we assume the function k to be increasing in the drug dose c. The function $p(y,s) \geq 0$ represents the cell proliferation rate, which we define as

$$p(y, s(t, \mathbf{x})) = f(y) + r(y, s(t, \mathbf{x})). \tag{5}$$

The function $f(y)$ is the proliferation rate under hypoxic conditions and is, therefore, an increasing function of the phenotypic state y [33]. The function $r(y, s)$ is decreasing in the phenotypic state y and increasing in the oxygen concentration s, since it models the rate of cell proliferation in oxygenated environments [14]. In this paper we consider

$$f(y) = \zeta \left[1 - (1-y)^2\right], \tag{6}$$

$$r(y, s(t, \mathbf{x})) = \gamma_s \frac{s(t, \mathbf{x})}{\alpha_s + s(t, \mathbf{x})} \left(1 - y^2\right), \tag{7}$$

$$k(y, c(t, \mathbf{x})) = \gamma_c \frac{c(t, \mathbf{x})}{\alpha_c + c(t, \mathbf{x})} \, (1 - y)^2. \tag{8}$$

These definitions satisfy the generic properties listed above and ensure analytical tractability of the model. The definitions (7) and (8) rely on the assumption that the consumption of oxygen and cytotoxic drug is governed by Michaelis-Menten kinetics with constants $\alpha_s > 0$ and $\alpha_c > 0$, respectively [22, 24]. The parameter $\gamma_c > 0$ is the maximum cell death rate induced by the cytotoxic drug. The parameters $\zeta > 0$ and $\gamma_s > 0$ represent the maximum proliferation rate under hypoxic conditions and in oxygenated environments, respectively. Previous empirical studies suggest that cancer cells inhabiting hypoxic regions in solid tumours proliferate more slowly than cells populating oxygenated regions [27, 31, 34]. In our modelling framework this observation is captured by the additional assumption $\zeta \ll \gamma_s$.

Dynamics of abiotic factors

The abiotic factors (*i.e.*, oxygen and cytotoxic drug) diffuse in space, decay and are consumed by cells. We note that the dynamics of abiotic factors is faster than cellular proliferation and death [35, 36]. From a mathematical viewpoint, this means that we can assume oxygen and the cytotoxic drug to be in quasi-stationary equilibrium. Under these assumptions, the dynamics of the functions $s(t,\mathbf{x})$ and $c(t,\mathbf{x})$ are described by the following elliptic PDEs that are coupled to the IDE (3)

$$\beta_s \Delta s(t,\mathbf{x}) = \eta_s \int_0^1 r\big(y, s(t,\mathbf{x})\big) n(t,\mathbf{x},y)\,\mathrm{d}y + \lambda_s s(t,\mathbf{x}), \tag{9}$$

$$\beta_c \Delta c(t,\mathbf{x}) = \eta_c \int_0^1 k\big(y, c(t,\mathbf{x})\big) n(t,\mathbf{x},y)\,\mathrm{d}y + \lambda_c c(t,\mathbf{x}). \tag{10}$$

In the above equations, the parameters $\beta_s > 0$ and $\beta_c > 0$ represent the diffusion constants of oxygen and the cytotoxic drug. The parameters $\eta_s > 0$ and $\eta_c > 0$ are the scaling factors for the consumption rate of abiotic factors by cells in the tumour. The parameters $\lambda_s > 0$ and $\lambda_c > 0$ represent the decay rates of oxygen and the cytotoxic drug. Focussing on the biological scenario in which the concentrations of abiotic factors in the medium surrounding the tumour are constant in time, we make use of the following boundary conditions for (9) and (10)

$$s(\cdot,\mathbf{x}) = S(\mathbf{x}) \quad \text{and} \quad c(\cdot,\mathbf{x}) = C(\mathbf{x}), \quad \mathbf{x} \in \partial\Omega. \tag{11}$$

The functions $S(\mathbf{x})$ and $C(\mathbf{x})$ model the concentrations of oxygen and cytotoxic drug on the tumour boundary $\partial\Omega$.

Table 1. Parameter values used to perform numerical simulations

Parameter	Biological meaning	Value	Reference
α_c	Michaelis-Menten constant of cytotoxic drug	$2 \times 10^{-6}\ g\,cm^{-3}$	[22,37]
α_s	Michaelis-Menten constant of oxygen	$1.5 \times 10^{-7}\ g\,cm^{-3}$	[38]
β_c	Diffusion coefficient of cytotoxic drug	$5 \times 10^{-6}\ cm^2\,s^{-1}$	[22,39]
β_s	Diffusion coefficient of oxygen	$2 \times 10^{-5}\ cm^2\,s^{-1}$	[40]
γ_c	Maximum cell death rate induced by cytotoxic drug	$1.8 \times 10^{-4}\ s^{-1}$	[22,37]
γ_s	Maximum cell proliferation rate in oxygenated environments	$1 \times 10^{-5}\ s^{-1}$	[24,38]
ζ	Maximum cell proliferation rate under hypoxic conditions	$1 \times 10^{-6}\ s^{-1}$	[30]
d	Rate of cell death due to competition for space	$2 \times 10^{-14}\ cm^3\,s^{-1}\,cell^{-1}$	[41]
η_c	Scaling factor for cell consumption of cytotoxic drug	$4 \times 10^{-12}\ g\,cell^{-1}$	[22,37]
η_s	Scaling factor for cell consumption of oxygen	$2 \times 10^{-12}\ g\,cell^{-1}$	[38]
λ_c	Decay rate of cytotoxic drug	$0.1\ s^{-1}$	[42]
λ_s	Decay rate of oxygen	$0.3\ s^{-1}$	[23]
ρ_0	Reference value for the local cell density	$10^9\ cells\,cm^{-3}$	[41]
s_0	Reference value for the local concentration of oxygen	$6.3996 \times 10^{-7}\ g\,cm^{-3}$	[43]
c_0	Reference value for the local concentration of cytotoxic drug	$10^{-5}\ g\,cm^{-3}$	[22]

Formal analysis of phenotypic selection

To obtain an analytical description of phenotypic selection, we assume that all possible phenotypic variants exist in the tumour at time $t = 0$, *i.e.*, we set $n(0, \mathbf{x}, y) > 0$ for all $\mathbf{x} \in \Omega$ and all $y \in [0, 1]$. Additionally, we assume that the number of cells in the tumour is bounded above and below. Given this scenario, for every position $\mathbf{x} \in \Omega$, the local cell density at equilibrium $\overline{\rho}(\mathbf{x})$ satisfies the following condition

$$\max_{y \in [0,1]} R\big(y, \overline{\rho}(\mathbf{x}), \overline{s}(\mathbf{x}), \overline{c}(\mathbf{x})\big) = 0,$$

where $\overline{s}(\mathbf{x})$ and $\overline{c}(\mathbf{x})$ stand for the steady-state distributions of oxygen and cytotoxic drug, respectively. Since the fitness landscape R is a monotonically decreasing function of the local number of cells, for every $\mathbf{x}$, there is a unique value of $\overline{\rho}(\mathbf{x})$ that satisfies the above relation. Moreover, given Eqs. (6)-(8), the fitness landscape R is a strictly concave function of y for all values of $\overline{\rho}(\mathbf{x})$, $\overline{s}(\mathbf{x})$ and $\overline{c}(\mathbf{x})$. This implies that, for all values of $\mathbf{x}$, there exists one single phenotypic state $\overline{y}(\mathbf{x})$ which maximises the fitness landscape R at equilibrium. Therefore, for each $\mathbf{x}$ there is a unique dominant phenotypic state $\overline{y}(\mathbf{x})$ (*i.e.*, at each position $\mathbf{x}$ in the tumour, the equilibrium phenotypic distribution is unimodal). Given the phenotypic state $\overline{y}(\mathbf{x})$, the following conditions are simultaneously satisfied

$$R\big(\overline{y}(\mathbf{x}), \overline{\rho}(\mathbf{x}), \overline{s}(\mathbf{x}), \overline{c}(\mathbf{x})\big) = \max_{y \in [0,1]} R\big(y, \overline{\rho}(\mathbf{x}), \overline{s}(\mathbf{x}), \overline{c}(\mathbf{x})\big) = 0$$

and

$$\frac{\partial R}{\partial y}\big(\overline{y}(\mathbf{x}), \overline{\rho}(\mathbf{x}), \overline{s}(\mathbf{x}), \overline{c}(\mathbf{x})\big) = 0.$$

Together, the above considerations allow us to conclude that, given $\overline{s}(\mathbf{x})$ and $\overline{c}(\mathbf{x})$, there exists a unique pair $(\overline{\rho}(\mathbf{x}), \overline{y}(\mathbf{x}))$ which solves the following system of equations

$$\begin{cases} R\big(\overline{y}(\mathbf{x}), \overline{\rho}(\mathbf{x}), \overline{s}(\mathbf{x}), \overline{c}(\mathbf{x})\big) = 0, \\ \\ \dfrac{\partial R}{\partial y}\big(\overline{y}(\mathbf{x}), \overline{\rho}(\mathbf{x}), \overline{s}(\mathbf{x}), \overline{c}(\mathbf{x})\big) = 0. \end{cases} \tag{12}$$

For every position $\mathbf{x} \in \Omega$, the pair $\big(\overline{\rho}(\mathbf{x}), \overline{y}(\mathbf{x})\big)$ characterises the local cell density and the dominant phenotypic state at equilibrium. The formal arguments presented above are consistent with the asymptotic analysis recently developed by Mirrahimi and Perthame for a system of equations modelling selection dynamics in a population structured by a phenotypic trait and a 1D spatial variable [44].

Solving the system given by (12) we obtain

$$\overline{\rho}(\mathbf{x}) = \frac{1}{d}\left[A_{\overline{s}}(\mathbf{x}) - A_{\overline{c}}(\mathbf{x}) + \frac{\Big(\zeta + A_{\overline{c}}(\mathbf{x})\Big)^2}{\zeta + A_{\overline{s}}(\mathbf{x}) + A_{\overline{c}}(\mathbf{x})}\right] \tag{13}$$

and

$$\overline{y}(\mathbf{x}) = \frac{\zeta + A_{\overline{c}}(\mathbf{x})}{\zeta + A_{\overline{s}}(\mathbf{x}) + A_{\overline{c}}(\mathbf{x})}, \tag{14}$$

where

$$A_{\overline{s}}(\mathbf{x}) = \gamma_s \frac{\overline{s}(\mathbf{x})}{\alpha_s + \overline{s}(\mathbf{x})} \quad \text{and} \quad A_{\overline{c}}(\mathbf{x}) = \gamma_c \frac{\overline{c}(\mathbf{x})}{\alpha_c + \overline{c}(\mathbf{x})}.$$

Here, (13) and (14) demonstrate that the local cell density $\overline{\rho}$ and the phenotypic state $\overline{y}$ which maximises the cellular fitness at position $\mathbf{x}$ are determined by the concentration of oxygen $\overline{s}$ and cytotoxic drug $\overline{c}$ at the same position. This is illustrated by the heat maps in Fig. 1, which show how, for the parameter values listed in Table 1, the values of $\overline{\rho}$ and $\overline{y}$ vary as functions of $\overline{s}$ and $\overline{c}$.

Together, these results suggest that local variations of abiotic factors in the tumour microenvironment determine spatial variations of selected phenotypic variants and cell densities.

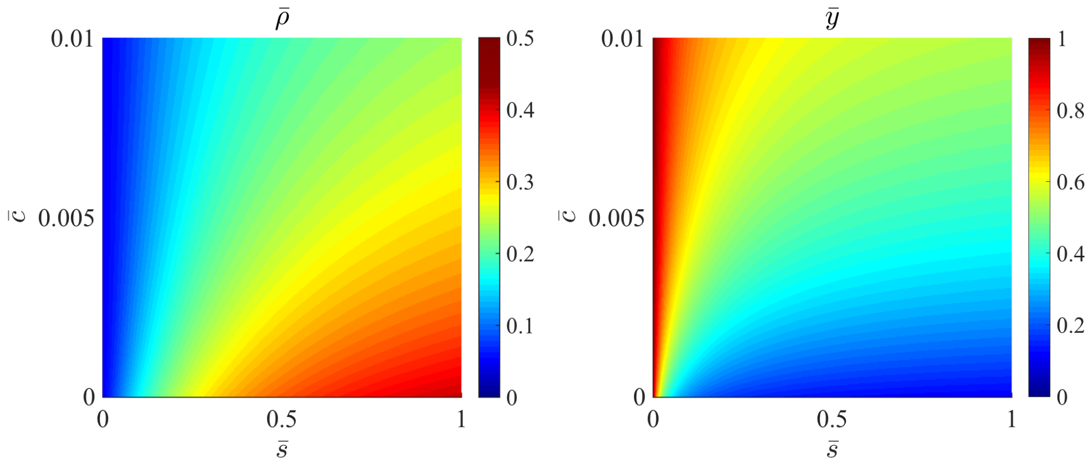

Figure 1. Plot of the local cell density $\overline{\rho}$ and the dominant phenotypic state $\overline{y}$ at equilibrium as functions of the local concentration of oxygen $\overline{s}$ and cytotoxic drug $\overline{c}$. The quantities $\overline{\rho}$, $\overline{s}$ and $\overline{c}$ are scaled by the reference values ρ_0, s_0 and c_0 given in Table 1.

Specifically, lower values of the oxygen concentration $\overline{s}$ and higher values of the drug concentration $\overline{c}$ correspond to higher values of the phenotypic state $\overline{y}$ and lower values of the local cell density $\overline{\rho}$. Biologically, this means that local environments hostile to highly proliferative cells (*i.e.*, environments characterised by lower oxygen availability and higher concentration of the cytotoxic agent) promote the selection of cells characterised by higher levels of expression of the hypoxia-responsive gene, which in turn leads to smaller cell numbers. On the contrary, higher values of $\overline{s}$ and lower values of $\overline{c}$ correspond to lower values of $\overline{y}$ and higher values of $\overline{\rho}$. Biologically, this means that highly proliferative cells are selected for in regions with higher oxygen and lower drug concentration, which in turn leads to larger cell densities.

Numerical solutions

We integrate the formal results established in the previous section with numerical simulations of the coupled system given by Eqs. (3), (9) and (10). First, we consider the case where the spatial domain Ω is an *in silico* tumour spheroid. Second, we consider the case where Ω corresponds to the three dimensional geometry of an *in vivo* human hepatic tumour, imaged using 3D computerised tomography. The image data were obtained from the 3D-IRCADb-01 database (http://www.ircad.fr/).

For the numerical simulations, we use the parameter values from the existing literature which are listed in Table 1. Further details of numerical simulations are provided as SI. In particular, a complete description of the numerical methods used in this work can be found in SI Appendix C. Primarily, we report here on results obtained under the assumption that the tumour is avascular and the concentrations of oxygen and cytotoxic drug on the boundary $\partial\Omega$ are constant (*i.e.*, $S(\mathbf{x}) = s_0$ and $C(\mathbf{x}) = c_0$ for all $\mathbf{x} \in \partial\Omega$). For the sake of completeness, we performed additional numerical simulations both in the case where abiotic factors are non-uniformly distributed on the boundary and in the case where blood vessels are enclosed within the tumour mass. The results obtained are presented and discussed at the end of this section.

In silico tumour spheroid simulations

The results obtained with and without the cytotoxic drug are presented in Fig. 2, where the local concentrations of abiotic factors, the local mean phenotypic state and the local cell density at equilibrium are shown.

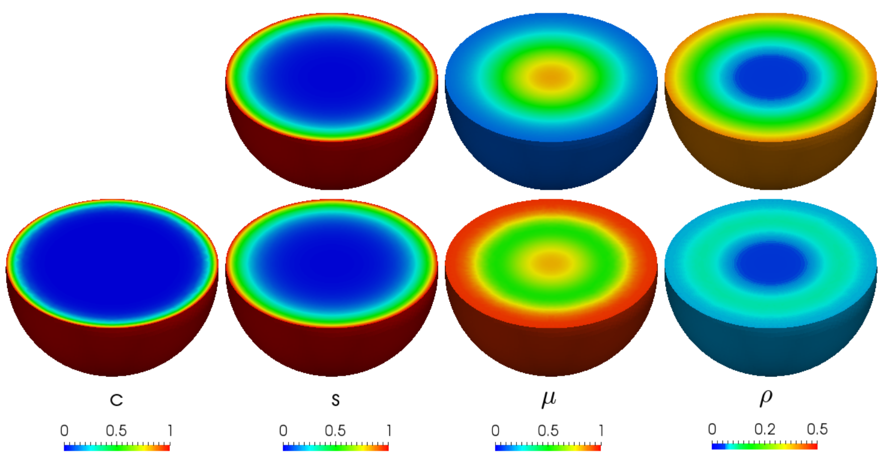

Figure 2. Plots of the local concentration of cytotoxic drug $c(t, \mathbf{x})$, the local concentration of oxygen $s(t, \mathbf{x})$, the local mean cell phenotypic state $\mu(t, \mathbf{x})$ and the local cell density $\rho(t, \mathbf{x})$ at $t = 70$ days [*i.e.*, close to the steady state of Eqs. (3), (9) and (10)] in an *in silico* tumour spheroid of radius $800\mu m$. The top and bottom rows refer to the cases when the cytotoxic drug is absent and present, respectively. For visualisation, only the bottom half of the spheroid is shown. The quantities c, s and ρ are scaled by the reference values c_0, s_0 and ρ_0 given in Table 1.

The concentrations of oxygen and cytotoxic drug, when present, decrease monotonically from the edge to the centre of the spheroid. As a consequence, in the absence of drug (*vid.* top row of Fig. 2), the local cell density decays radially with maximum value on the spheroid boundary. We observe the formation of a necrotic core, with very few living cells, surrounded by a hypoxic region, then by a more densely populated rim with more living cells present. Biologically, our results suggest that the outer part of the spheroid becomes colonised by highly proliferative cells, while slow-proliferating cells with a hypoxic phenotype are selected for in the interior of the spheroid. Accordingly, the local mean phenotypic state is a radially decreasing function from the centre to the boundary of the spheroid.

When the cytotoxic drug is present (*vid.* bottom row of Fig. 2), the number of living cells is consistently reduced throughout the whole tumour spheroid. The selective pressure exerted by the drug drives the mean phenotypic state towards drug-resistance. Moreover, the local cell density and the local mean phenotypic state are no longer monotonic functions of the distance from the centre of the spheroid. In this case, the density of living cells is close to zero at both the boundary and the core of the tumour. Therefore, most of the surviving cells are found in a thin band in the interior of the spheroid where the local mean phenotypic state attains its minimum.

Both with and without the cytotoxic drug, at each position $\mathbf{x}$ the phenotypic distribution $n(t, \mathbf{x}, y)$ has a Gaussian-like profile (*vid.* Fig. S1 in the SI); therefore, the local mean phenotypic state coincides with the locally dominant phenotypic state. To this end, Movie S1 in the SI demonstrates that after a short time period of transient behaviour, the local cell density $\rho(t, \mathbf{x})$ and the local mean phenotypic state $\mu(t, \mathbf{x})$ converge, respectively, to the equilibrium values of the local cell density $\overline{\rho}(\mathbf{x})$, given by (13), and of the dominant phenotypic state $\overline{y}(\mathbf{x})$, given by (14).

In vivo human hepatic tumour simulations

Figure 3 illustrates the computerised tomography scan of the human liver tumour which we selected as the spatial domain Ω.

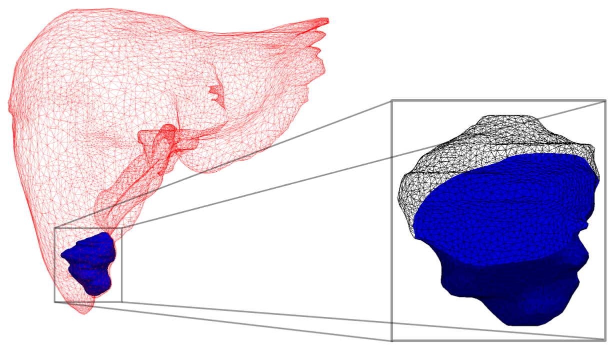

Figure 3. Computerised tomography scan of a human tumour (blue) shown *in situ* within the liver (red). The maximum diameter of the tumour is approximatively $3200\mu m$. The inset shows a magnification of the tumour with a portion made transparent, as in Fig. 4, in order to visualise the tumour bulk.

Our numerical simulations indicate that the spatial distributions of cells, oxygen and cytotoxic drug as well as the spatial patterns of phenotypic selection for the hepatic tumour are qualitatively similar to those observed in the *in silico* tumour spheroid (compare the results in Fig. 3 with the results of Fig. 2, and the results of Movie S1 with the results displayed by Movie S2 in the SI).

Effects of tumour vasculature and non-uniform boundary distributions of abiotic factors

The results presented in Fig. 5 and Fig. 6 show that similar conclusions apply both to the case with tumour vasculature and to the case with non-uniform boundary distributions of abiotic factors. Specifically, when the cytotoxic drug is not present, highly proliferative cells are selected for in the tumour areas where oxygen concentration is higher. Conversely, poorly oxygenated regions are colonised by slow-proliferating cells which express hypoxic phenotypes. These hypoxic cells, characterised by lower levels of drug-sensitivity, become dominant within the tumour upon delivery of the cytotoxic drug.

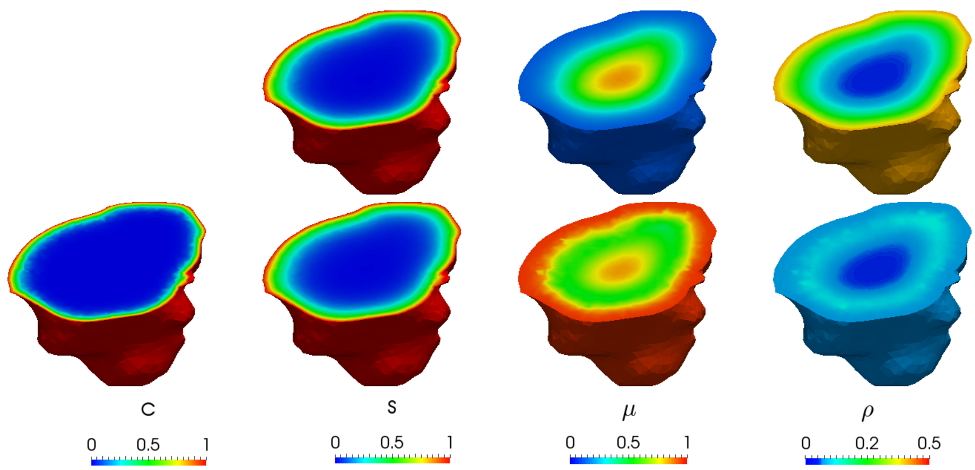

Figure 4. Plots of the local concentration of cytotoxic drug $c(t, \mathbf{x})$, the local concentration of oxygen $s(t, \mathbf{x})$, the local mean cell phenotypic state $\mu(t, \mathbf{x})$ and the local cell density $\rho(t, \mathbf{x})$ at $t = 70$ days [*i.e.*, close to the steady state of Eqs. (3), (9) and (10)] in the human hepatic tumour of Fig. 3. The top and bottom row refer to the cases when the cytotoxic drug is absent and present, respectively. For better visualisation, only a portion of the tumour is shown. The quantities c, s and ρ are scaled by the reference values c_0, s_0 and ρ_0 given in Table 1.

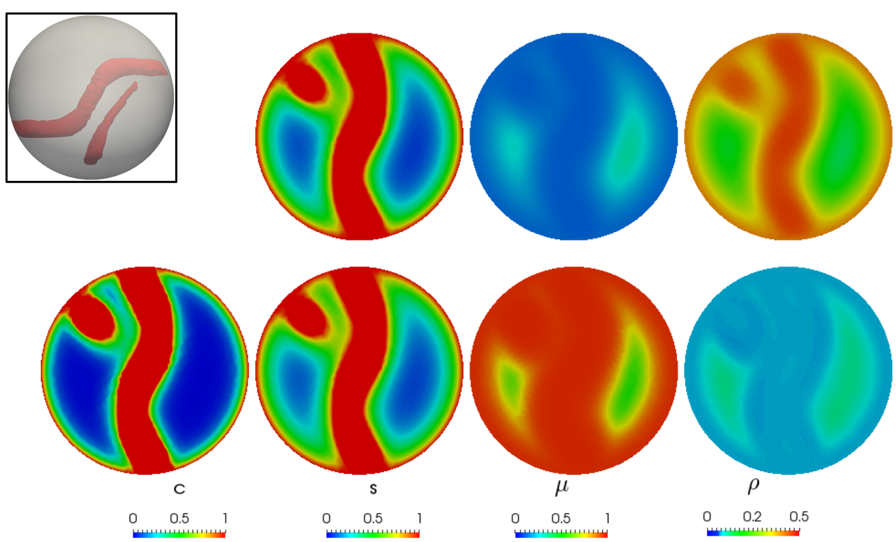

Figure 5. Plots of the local concentration of cytotoxic drug $c(t, \mathbf{x})$, the local concentration of oxygen $s(t, \mathbf{x})$, the local mean cell phenotypic state $\mu(t, \mathbf{x})$ and the local cell density $\rho(t, \mathbf{x})$ at $t = 70$ days [*i.e.*, close to the steady state of Eqs. (3), (9) and (10)] in a slice of the *in silico* tumour spheroid shown in the inset. The top and bottom row refer to the cases when the cytotoxic drug is absent and present, respectively. The quantities c, s and ρ are scaled by the reference values c_0, s_0 and ρ_0 given in Table 1.

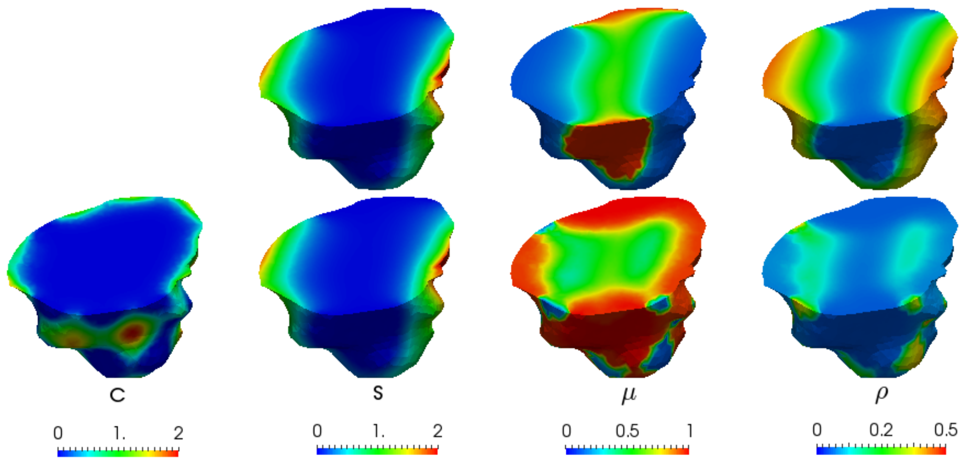

Figure 6. Plots of the local concentration of cytotoxic drug $c(t, \mathbf{x})$, the local concentration of oxygen $s(t, \mathbf{x})$, the local mean cell phenotypic state $\mu(t, \mathbf{x})$ and the local cell density $\rho(t, \mathbf{x})$ at $t = 70$ days [*i.e.*, close to the steady state of Eqs. (3), (9) and (10)] in the human hepatic tumour of Fig. 3. These results have been obtained in the case of spatially varying boundary conditions for the abiotic factors. The top and bottom row displays the results obtained in the absence and in the presence of cytotoxic drug, respectively. For better visualisation, only the bottom half of the tumour is shown. The quantities c, s and ρ are scaled by the reference values c_0, s_0 and ρ_0 given in Table 1.

Discussion

Our analysis and numerical simulations support the hypothesis that spatial variations in oxygen levels can foster the emergence of phenotypic heterogeneity by promoting the creation of distinct local niches within the same tumour. Our model predicts that well-oxygenated regions of the tumour – such as the tumour periphery and areas close to blood vessels – will be densely populated by highly proliferative cancer cells characterised by higher oxygen uptake. Conversely, hypoxic cells with lower proliferation rates colonise tumour regions hostile to fast-proliferating cells – such as the inner regions of the tumour where oxygen concentration is lower.

Our modelling framework offers a plausible theoretical basis for recent experimental results suggesting that the periphery and the centre of solid tumours represent distinct ecological niches [27, 31, 45–47]. Furthermore, our findings agree with observations made in mathematical modelling and experimental studies [31, 48–51] which suggest that hypoxia favours the selection for cancer cells resistant to cytotoxic therapy prior to treatment. Consequently, this facilitates the development of resistance following drug exposure.

Our analysis and numerical simulations also address the open question of how phenotypic heterogeneity in a solid tumour changes under cytotoxic therapy. Our results complement those of Robertson-Tessi *et al.* [52] by demonstrating that cytotoxic agents decrease the number of living cancer cells and select for more resistant phenotypic variants throughout the whole tumour. In particular, since cytotoxic drugs kill more proliferative cells in regions of the tumour with higher oxygen concentration, the drug exposure removes the selective barrier limiting the growth of less proliferative and more resistant cells. This reduces drug efficacy, and ultimately leads to poor treatment outcomes and low patient survival rates [53–55].

In summary, our mathematical study highlights the role that the spatial distribution of abiotic components in the tumour microenvironment play in mediating phenotypic heterogeneity in solid tumours. Our results strongly support the need for spatial data when performing phenotypic profiling of solid tumours, as single tumour biopsies are unlikely to fully represent the complete phenotypic landscape of the tumour [4–7, 56].

Histological analyses indicate that solid tumours contain cancer cells with a wide spectrum of gene expression. However, our theoretical work provides support for the ideas proposed by Alfarouk *et al.* [14], who have noted that the phenotypes of cancer cells result, to an extent, from predictable spatial gradients in the concentrations of abiotic factors which can be mapped out via non-invasive imaging techniques [57]. This may open up new avenues of research for exploiting ecological principles to design innovative therapeutic protocols according to adaptive therapy [58, 59].

Additional strengths of the present study are that the parameter values used to perform numerical simulations come from existing literature, and the outcomes of our formal analysis are characterised by broad structural stability under parameter changes. Our framework can accommodate parameter values for any solid tumour and the method we have used to construct numerical solutions of the model is applicable to arbitrary geometries. Therefore, while we performed numerical simulations on the geometry of a given *in vivo* human hepatic tumour as an illustrative example, our *in silico* approach can be applied to studying phenotypic selection between cancer cells in a wide range of neoplasms.

Finally, while we have assumed multiple phenotypic variants to be present in the tumour from the beginning of simulations and we have considered the tumour size to remain constant over time, the modelling framework presented here can be extended to incorporate mutations and epimutations [20, 21] as well as growing tumour spatial domains [60–64]. Given the robustness and structural stability of our results, we expect the main conclusions of this work to hold even after the inclusion of these additional layers of biological complexity.

References

1. Bhang HC, Ruddy DA, Radhakrishna VK, Caushi JX, Zhao R, Hims MM, et al., Studying clonal dynamics in response to cancer therapy using high-complexity barcoding. Nature medicine (2015) 21: 440–448.

2. Vermeulen L, Morrissey E, van der Heijden M, Nicholson AM, Sottoriva A, Buczacki S, et al., Defining stem cell dynamics in models of intestinal tumor initiation. Science (2013) 342: 995–998.

3. Wang Y, Waters J, Leung ML, Unruh A, Roh W, Shi X, et al., Clonal evolution in breast cancer revealed by single nucleus genome sequencing. Nature (2014) 512: 155–160.

4. Ding L, Ellis MJ, Li S, Larson DE, Chen K, Wallis JW, et al., Genome remodelling in a basal-like breast cancer metastasis and xenograft. Nature (2010) 464: 999–1005.

5. Zhang J, Fujimoto J, Zhang J, Wedge DC, Song X, Zhang J, et al., Intratumor heterogeneity in localized lung adenocarcinomas delineated by multiregion sequencing. Science (2014) 346: 256–259.

6. Yap TA, Gerlinger M, Futreal PA, Pusztai L, Swanton C, Intratumor heterogeneity: seeing the wood for the trees. Science Translational Medicine (2012) 4: 127ps10–127ps10.

7. Martinez P, Birkbak NJ, Gerlinger M, McGranahan N, Burrell RA, Rowan AJ, et al., Parallel evolution of tumour subclones mimics diversity between tumours. J Pathol (2013) 230: 356–364.

8. Gerlinger M, Rowan AJ, Horswell S, Larkin J, Endesfelder D, Gronroos E, et al., Intratumor heterogeneity and branched evolution revealed by multiregion sequencing. New England Journal of Medicine (2012) 366: 883–892.

9. Marusyk A, Almendro V, Polyak K, Intra-tumour heterogeneity: a looking glass for cancer? Nature Reviews Cancer (2012) 12: 323–334.

10. Pribluda A, Cecile C, Jackson EL, Intratumoral heterogeneity: from diversity comes resistance. Clinical Cancer Research (2015) 21: 2916–2923.

11. Merlo LM, Pepper JW, Reid BJ, Maley CC, Cancer as an evolutionary and ecological process. Nature Reviews Cancer (2006) 6: 924–935.

12. Greaves M, Maley CC, Clonal evolution in cancer. Nature (2012) 481: 306–313.

13. Pienta KJ, McGregor N, Axelrod R, Axelrod DE, Ecological therapy for cancer: defining tumors using an ecosystem paradigm suggests new opportunities for novel cancer treatments. Translational Oncology (2008) 1: 158–164.

14. Alfarouk KO, Ibrahim ME, Gatenby RA, Brown JS, Riparian ecosystems in human cancers. Evolutionary Applications (2013) 6: 46–53.

15. Gillies RJ, Verduzco D, Gatenby RA, Evolutionary dynamics of carcinogenesis and why targeted therapy does not work. Nature Reviews Cancer (2012) 12: 487–493.

16. Meads MB, Gatenby RA, Dalton WS, Environment-mediated drug resistance: a major contributor to minimal residual disease. Nature Reviews Cancer (2009) 9: 665–674.

17. Trédan O, Galmarini CM, Patel K, Tannock IF, Drug resistance and the solid tumor microenvironment. Journal of the National Cancer Institute (2007) 99: 1441–1454.

18. Chisholm RH, Lorenzi T, Lorz A, Larsen AK, De Almeida LN, Escargueil A, et al., Emergence of drug tolerance in cancer cell populations: an evolutionary outcome of selection, nongenetic instability, and stress-induced adaptation. Cancer Research (2015) 75: 930–939.

19. Delitala M, Lorenzi T, A mathematical model for the dynamics of cancer hepatocytes under therapeutic actions. Journal of Theoretical Biology (2012) 297: 88–102.

20. Lorenzi T, Chisholm RH, Clairambault J, Tracking the evolution of cancer cell populations through the mathematical lens of phenotype-structured equations. Biology Direct (2016) 11: 43.

21. Lorz A, Lorenzi T, Hochberg ME, Clairambault J, Perthame B, Populational adaptive evolution, chemotherapeutic resistance and multiple anti-cancer therapies. ESAIM: Mathematical Modelling and Numerical Analysis (2013) 47: 377–399.

22. Norris E, King JR, Byrne HM, Modelling the response of spatially structured tumours to chemotherapy: Drug kinetics. Mathematical and Computer Modelling (2006) 43: 820–837.

23. Macklin P, McDougall S, Anderson AR, Chaplain MA, Cristini V, Lowengrub J, Multiscale modelling and nonlinear simulation of vascular tumour growth. Journal of Mathematical Biology (2009) 58: 765–798.

24. Ward JP, King J, Mathematical modelling of avascular-tumour growth. Mathematical Medicine and Biology (1997) 14: 39–69.

25. Fu F, Nowak MA, Bonhoeffer S, Spatial heterogeneity in drug concentrations can facilitate the emergence of resistance to cancer therapy. PLoS Computational Biology (2015) 11: e1004142.

26. Lorz A, Lorenzi T, Clairambault J, Escargueil A, Perthame B, Modeling the effects of space structure and combination therapies on phenotypic heterogeneity and drug resistance in solid tumors. Bulletin of Mathematical Biology (2015) 77: 1–22.

27. Lloyd MC, Cunningham JJ, Bui MM, Gillies RJ, Brown JS, Gatenby RA, Darwinian dynamics of intratumoral heterogeneity: not solely random mutations but also variable environmental selection forces. Cancer Research (2016) 76: 3136–3144.

28. Strese S, Fryknäs M, Larsson R, Gullbo J, Effects of hypoxia on human cancer cell line chemosensitivity. BMC Cancer (2013) 13: 1.

29. Zhao Y, Butler EB, Tan M, Targeting cellular metabolism to improve cancer therapeutics. Cell Death & Disease (2013) 4: e532.

30. Gordan JD, Bertout JA, Hu CJ, Diehl JA, Simon MC, Hif-2α promotes hypoxic cell proliferation by enhancing c-myc transcriptional activity. Cancer Cell (2007) 11: 335–347.

31. Brown JM, Giaccia AJ, The unique physiology of solid tumors: opportunities (and problems) for cancer therapy. Cancer Research (1998) 58: 1408–1416.

32. Durand RE, Raleigh JA, Identification of nonproliferating but viable hypoxic tumor cells in vivo. Cancer Research (1998) 58: 3547–3550.

33. Xia T, Cheng H, Zhu Y, Knockdown of hypoxia-inducible factor-1 alpha reduces proliferation, induces apoptosis and attenuates the aggressive phenotype of retinoblastoma weri-rb-1 cells under hypoxic conditions. Annals of Clinical & Laboratory Science (2014) 44: 134–144.

34. Brown JM, Wilson WR, Exploiting tumour hypoxia in cancer treatment. Nature Reviews Cancer (2004) 4: 437–447.

35. Jacqueline C, Biro PA, Beckmann C, Moller AP, Renaud F, Sorci G, et al., Cancer: A disease at the crossroads of trade-offs. Evol Appl (2017) 10: 215–225.

36. Walther V, Hiley CT, Shibata D, Swanton C, Turner PE, Maley CC, Can oncology recapitulate paleontology? Lessons from species extinctions. Nat Rev Clin Oncol (2015) 12: 273–285.

37. Kwok T, Twentyman P, The response to cytotoxic drugs of emt6 cells treated either as intact or disaggregated spheroids. British Journal of Cancer (1985) 51: 211.

38. Casciari JJ, Sotirchos SV, Sutherland RM, Variations in tumor cell growth rates and metabolism with oxygen concentration, glucose concentration, and extracellular ph. Journal of Cellular Physiology (1992) 151: 386–394.

39. Levin VA, Patlak CS, Landahl HD, Heuristic modeling of drug delivery to malignant brain tumors. Journal of Pharmacokinetics and Biopharmaceutics (1980) 8: 257–296.

40. Hlatky L, Alpen E, Two-dimensional diffusion limited system for cell growth. Cell Proliferation (1985) 18: 597–611.

41. Li CK, The glucose distribution in 9l rat brain multicell tumor spheroids and its effect on cell necrosis. Cancer (1982) 50: 2066–2073.

42. Calabresi P, Schein PS, Rosenberg SA (1985) Medical oncology: basic principles and clinical management of cancer. MacMillan Pub. Co., New York, NY.

43. Kumosa LS, Routh TL, Lin JT, Lucisano JY, Gough DA, Permeability of subcutaneous tissues surrounding long-term implants to oxygen. Biomaterials (2014) 35: 8287–8296.

44. Mirrahimi S, Perthame B, Asymptotic analysis of a selection model with space. Journal de Mathématiques Pures et Appliquées (2015) 104: 1108–1118.

45. Hoefflin R, Lahrmann B, Warsow G, Hübschmann D, Spath C, Walter B, et al., Spatial niche formation but not malignant progression is a driving force for intratumoural heterogeneity. Nature Communications (2016) 7.

46. Tannock I, The relation between cell proliferation and the vascular system in a transplanted mouse mammary tumour. British Journal of Cancer (1968) 22: 258.

47. Zhang X, Fryknäs M, Hernlund E, Fayad W, De Milito A, Olofsson MH, et al., Induction of mitochondrial dysfunction as a strategy for targeting tumour cells in metabolically compromised microenvironments. Nature Communications (2014) 5.

48. Adamski J, Price A, Dive C, Makin G, Hypoxia–induced cytotoxic drug resistance in osteosarcoma is independent of hif-1alpha. PloS One (2013) 8: e65304.

49. Powathil GG, Gordon KE, Hill LA, Chaplain MA, Modelling the effects of cell-cycle heterogeneity on the response of a solid tumour to chemotherapy: biological insights from a hybrid multiscale cellular automaton model. Journal of Theoretical Biology (2012) 308: 1–19.

50. Sullivan R, Paré GC, Frederiksen LJ, Semenza GL, Graham CH, Hypoxia-induced resistance to anticancer drugs is associated with decreased senescence and requires hypoxia-inducible factor-1 activity. Molecular Cancer Therapeutics (2008) 7: 1961–1973.

51. Wartenberg M, Ling FC, Müschen M, Klein F, Acker H, Gassmann M, et al., Regulation of the multidrug resistance transporter p-glycoprotein in multicellular tumor spheroids by hypoxia-inducible factor (hif-1) and reactive oxygen species. The FASEB Journal (2003) 17: 503–505.

52. Robertson-Tessi M, Gillies RJ, Gatenby RA, Anderson AR, Impact of metabolic heterogeneity on tumor growth, invasion, and treatment outcomes. Cancer Research (2015) 75: 1567–1579.

53. Sottoriva A, Spiteri I, Piccirillo SG, Touloumis A, Collins VP, Marioni JC, et al., Intratumor heterogeneity in human glioblastoma reflects cancer evolutionary dynamics. Proc Natl Acad Sci USA (2013) 110: 4009–4014.

54. Williams MJ, Werner B, Barnes CP, Graham TA, Sottoriva A, Identification of neutral tumor evolution across cancer types. Nat Genet (2016) 48: 238–244.

55. Jones AM, Mitter R, Springall R, Graham T, Winter E, Gillett C, et al., A comprehensive genetic profile of phyllodes tumours of the breast detects important mutations, intratumoral genetic heterogeneity and new genetic changes on recurrence. J Pathol (2008) 214: 533–544.

56. Schwarz RF, Ng CK, Cooke SL, Newman S, Temple J, Piskorz AM, et al., Spatial and temporal heterogeneity in high-grade serous ovarian cancer: a phylogenetic analysis. PLoS Med (2015) 12: e1001789.

57. Beerenwinkel N, Greenman CD, Lagergren J, Computational cancer biology: an evolutionary perspective. PLoS Computational Biology (2016) 12: e1004717.

58. Gatenby RA, Silva AS, Gillies RJ, Frieden BR, Adaptive therapy. Cancer Research (2009) 69: 4894–4903.

59. Ibrahim-Hashim A, Robertson-Tessi M, Enrizues-Navas P, Damaghi M, Balagurunathan Y, Wojtkowiak JW, et al., Defining cancer subpopulations by adaptive strategies rather than molecular properties provides novel insights into intratumoral evolution. Cancer Res (2017) .

60. Ambrosi D, Preziosi L, On the closure of mass balance models for tumor growth. Mathematical Models and Methods in Applied Sciences (2002) 12: 737–754.

61. Byrne HM, Chaplain M, Growth of necrotic tumors in the presence and absence of inhibitors. Mathematical Biosciences (1996) 135: 187–216.

62. Byrne H, Drasdo D, Individual-based and continuum models of growing cell populations: a comparison. Journal of Mathematical Biology (2009) 58: 657–687.

63. Lorenzi T, Lorz A, Perthame B, On interfaces between cell populations with different mobilities. Kinetic and Related Models (2017) 10: 299–311.

64. Perthame B, Quirós F, Vázquez JL, The hele–shaw asymptotics for mechanical models of tumor growth. Archive for Rational Mechanics and Analysis (2014) 212: 93–127.

Acknowledgements

The authors would like to thank Dana-Adriana Botesteanu for her helpful feedback and insightful comments and suggestions.

Competing interests

The authors declare that they have no competing interests.

Author's contributions

T.L, C.V. and A.L. formulated the model; M.A.J. coordinated the study; T.L. and C.V. performed mathematical study and critical analysis of the results; T.L., C.V., A.L. and M.A.J. wrote the paper.

Funding

CV wishes to acknowledge partial support from the European Union's Horizon 2020 research and innovation programme under the Marie Sklodowska-Curie grant agreement No 642866. AL was supported by King Abdullah University of Science and Technology (KAUST) baseline and start-up funds (BAS/1/1648-01-01 and BAS/1/1648-01-02). MAJC gratefully acknowledge support of EPSRC grant no. EP/N014642/1.